An Investigation on The Quality of Denoised Images

†Peter Ndajah, ‡Hisakazu Kikuchi, ‡Masahiro Yukawa, †Hidenori Watanabe, ‡Shogo Muramatsu

***Abstract*—The mean squared error (MSE) and its related metrics such as peak signal to noise ratio (PSNR), root mean squared error (RMSE) and signal to noise ratio (SNR) have been the basis for mathematically defined image quality measurement for a long time. These methods are all based on the MSE. Denoised image quality has also been traditionally measured in terms of the MSE or its derivatives. However, none of these metrics takes the structural fidelity of the image into account. We investigate the structural changes that occur during the denoising process and attempt to study an alternative metric for determining the quality of denoised images based on structural changes. We also show the shortcomings of the MSE-based image quality metrics.**

***Index Terms*—SSIM, MSE, TV, PSNR, Noise, Denoise, Metric**

I. Introduction

In this work we set out to determine if the traditional image quality metrics such as the mean square error actually give accurate measure of image quality improvement after denoising. We therefore explore the use of the MSE and the peak signal to noise ratio (PSNR) as error sensitivity metrics and structural similarity metric (SSIM) that measures the structural similarity of an image against a reference image. The structural similarity of a denoised image tells us how much of the original structure has been recovered after denoising. We then study the SSIM of the denoised image against the MSE and PSNR to determine different aspects of the image recovery process. However, the fact that the measurement metric should give an accurate estimation of the degree of restoration of the denoised image must be kept in mind. Traditionally, the error sensitivity approach has been used to measure the degree of recovery. But the question must be asked if this is in itself a sufficient tool to measure the quality of denoised images. The structure of an image makes us infer that the error sensitivity metrics have inadequacies in the manner in which they measure image quality in general. For one, they do not model the human visual system (HVS) adequately so that the aspects of image quality which they measure do not necessarily reflect the reality of the HVS. The ultimate aim of denoising an image is to render it more pleasing to the eye (HVS). The eye remains the best judge of image quality. For this reason, we need to use a metric that models the HVS as closely as possible. This is indeed a difficult task. The shortcoming of the error-sensitivity methods arise primarily in the assumptions made in the measuring process. For example, the assumption that the reference image is of perfect quality is a necessary assumption, otherwise no meaningful comparison of image quality can be made. But at the same time, it is assumed that the channels of the HVS have little or no interaction, which is not the case. The error sensitivity models work well for simple patterns but for patterns such as natural images where many simple patterns coincide at the same image location, the error sensitivity models do not give a very good approximation to the true quality of a denoised image.

We use the SSIM as an alternative metric to measure structural recovery after denoising. It is important to note that the structural distortion models measure different parameters of images from the error sensitivity models. We shall explore these differences and how they affect image quality.

†Graduate School of Science and Technology, Niigata University, 8050, Ikarashi 2-n-cho, Nishi-ku, Niigata, 950-2181, Japan. e-mail: ndajah@telecom0.eng.niigata-u.ac.jp..

‡Department of Electrical and Electronics Engineering, Niigata University, 8050, Ikarashi 2-n-cho, Nishi-ku, Niigata, 950-2181, Japan.

Manuscript received November 17, 2010; revised February 26, 2011.

II. Image Quality Measurement

There are basically two classes of objective quality assessment of images. The first are the mathematically defined measures such as the mean square error (MSE), peak signal to noise ratio (PSNR), root mean square error (RMSE) and signal to noise ratio (SNR). The second class of measurement methods depend on the characteristics of the human visual system (HVS) in an attempt to incorporate perceptual quality measures. Of the two methods the mathematically defined measures are most widely used. This is because of simplicity of implementation. Most error sensitivity methods are based on the mean square error (MSE). In most cases, they are equivalent metrics. The MSE is parameter free, inexpensive to compute and the samples in an image are assumed to be independent. The MSE offers a clear physical meaning. It measures the energy of the signal using the L^2-norm. Because of the reflexivity of the L^2 space, any transformation of the error energy is preserved isometrically in the dual space which is also an L^2 space. The L^2-norm is energy preserving.

The MSE is an old statistical tool and it was first used by C.F. Gauss to represent the statistical variance of the random samples. He also used it in the method of least squares. There are many other instances of the usefulness of the MSE. Historically, it has been used extensively for assessing a wide variety of imaging problems such as image compression, restoration, denoising, classification and reconstruction. The MSE is pervasive throughout the literature. It has been the de facto tool for signal strength comparison.

This wide acceptability of the MSE makes it very difficult to abandon. So even though there may be alternatives to the MSE, its use is not likely to diminish for some time to come.

But the error sensitivity models are not the only class of models suitable for measuring image quality. There are models based on the human visual system (HVS) that can accomplish the same purpose albeit using different criteria from the MSE-based methods. These models deal more with the perception of the human eye. A serious drawback of any error sensitivity model is that it treats all image degradations as some kind of error. But the human eye is well adapted to extract structural information from an image. The error sensitivity models do not capture this fact. Unfortunately, modeling the HVS has not known very good progress over the years. This could be directly attributed to our limited understanding of the HVS. However, it is generally known that the HVS

1. Has low-pass filter characteristics
2. Lacks color resolution
3. Shows sensitivity to motion
4. Exhibits integral face recognition characteristics
5. Is sensitive to structural distortion

The model we shall use takes the structural distortion into account to determine the quality of denoised images. The HVS has evolved to adapt its functions to extract useful structural information from natural scenes. Therefore, an image quality metric that aims to predict the evaluation behavior of the HVS will also need to be adapted to the properties of natural image signals. A distinct feature of natural images is that the image pixels(signals) exhibit strong dependencies among themselves. The greatest failure of the error sensitivity methods lies in the fact that they ignore the structural dependencies between image signal samples. This why its ability to provide an acceptable quality measure for denoised images is suspect.

In the past century, there has been considerable progress in increasing our depth of understanding the functions of the human perceptual system and developing mathematical models for its functions. However, our knowledge of human perception remains rudimentary. The most common approach to perception is by developing appropriate mathematical models for each functional perceptual component. These components form building blocks which are eventually integrated into a full system.

Denoising follows the same process. To measure the quality of a denoised image, we first need a mathematical model that denoises the image. Different denoising models have different denoising capabilities. Second, we need a mathematical model that tells us exactly how much the image has been recovered i.e. the degree of restoration. As we shall show, the error sensitivity methods do not tell the whole story.

The ultimate judge of image quality is the human eye and what is more important to the eye is the structural fidelity of a denoised image. The HVS is quite sensitive to structural information. How close the structure of a denoised image is to the reference image really does matter. For this reason we can say that the eye appeal of a denoised image is dependent on the accuracy of the structural information between the denoised image and its reference image.

Most HVS-based methods use some form of bottom-up approach. They simulate the functions of relevant components in the HVS and combine them together, with the goal that the combined system can predict the behavior of the overall HVS. The effectiveness of these methods depend on how much the HVS is understood and how accurately the simulation can be implemented. By contrast, straightforward structural approaches are based on a top-down philosophy, which starts from the top level–simulating the hypthesized functionality of the overall HVS. Top-down approaches sometimes lead to significantly simplified algorithms, but rely heavily on the accuracy of the underlying hypothesis. In particular, the basic assumption made by structural approaches is that the HVS is highly adapted to extract structural information from the visual scene, and therefore structural distortion measure should give good prediction of perceived image quality. Current experiments have demonstrated this to be the case.

The paradigm of structural image quality assessment is still new. The current approaches can be extended in many directions. Direct extensions include video quality assessment, colour image quality assessment and multiscale image quality assessment. Furhtermore, the SSIM index approach is quite encouraging not only because of its good image quality prediction accuracy, but also its simple formulation and low computational complexity. This simplicity makes it quite tractable. Consequently, the SSIM index, and other structurally-oriented image quality assessment algorithms have great potential to be used in the future development of image quality measurement. We give a comparison of the error-sensitivity methods and the structural distortion method and investigate the effect of each on the quality of denoised images.

III. Error Sensitivity Methods

The dominant error-sensitivity measurement tool has been the mean square error. There are variations of the MSE that are also in use as we mentioned. The MSE is used as a signal fidelity measure. The goal of signal fidelity measure is to compare two signals by providing a quantitative score to determine the level of error or distortion between them. The MSE between two signals **x** and **y** is

$$MSE(\mathbf{x},\mathbf{y}) = \frac{1}{N}\sum_{i=1}^{N}(x_i - y_i)^2 \tag{1}$$

The error signal $e_i = x_i - y_i$ is the difference between the original and distorted signal. More generally the error can be written in terms of the l_p-norm:

$$d_p(\mathbf{x},\mathbf{y}) = \left(\sum_{i=1}^{N}(x_i - y_i)\right)^{\frac{1}{p}} \tag{2}$$

which is called the Minkowski metric. The MSE is however usually expressed as the peak signal to noise ration (PSNR) measure

$$PSNR = 10\log_{10}\frac{L^2}{MSE} \tag{3}$$

where L is the dynamic range of allowable pixel intensities. For example, for an 8-bit per pixel image, $L = 2^8 - 1 = 255$. The error-sensitivity methods derive their effectiveness from

Fig. 1: Distorted Image Fidelity Measure

the Minkowski metric. The Minkowski metric is given as

$$\|E_p\| = \left(\sum_{i=1}^{N} |x_i - y_i|^p \right)^{\frac{1}{p}}. \quad (4)$$

$MSE = \frac{1}{N}\|E_p\|^p$ when $p = 2$. The Minkowski metric between the original image and the distorted image is always the same no matter what power of p is used. This is so even when the quality of the distorted images changes drastically. When $p = 2$, the Minkowski metric effectively becomes the means square error(MSE) metric. An implicit assumption of the Minkowski metric is that all signal samples are independent. For this reason its value remains the same even when there is a rearrangement of pixels in the image. The MSE is a special case of the Minkowski metric when $p = 2$. It is useful because when $p = 2$, the metric is a hilbert norm. The Hilbert space is reflexive and so the Hilbert space is the same as its dual space. This has the consequence of preserving energy in general. This is possible only when $p = 2$. In the Minkowski norm

$$E_p = \left(\sum_{i=1}^{N} |x_i - y_i|^p \right)^{\frac{1}{p}}$$

where x_i and y_i are the ith samples in the images $\mathbf{x}$ and $\mathbf{y}$ respectively, N is the number of image samples, and p refers to the degree of power. In the MSE, we refer to the error signal $e_i = x_i - y_i$ which is the difference between the original and distorted signals. The MSE may be regarded as a measure of signal quality. It is believed that the smaller the error is the closer the two images are in quality and that when the value of the MSE does not change the there is no possible change of quality between the two images. But as we will show through experimental results, this is not true.

Like we said earlier, the MSE is converted into a peak signal-to-noise ratio measure usually given as

$$PSNR = 10 \log_{10} \frac{L^2}{MSE}$$

where L is the dynamic range of allowable image pixel intensities. The PSNR differs in quality of measurement only when the images have different dynamic ranges, otherwise it contains no new information relative to the MSE [18]. The Minkowski metric does not respect the ordering and pattern of the signal samples. However it is known that pixel order carries important visual information in the image. This failure encourages us to examine other methods of image quality measurement based on other principles.

There are other relatives of the PSNR which deserve

mention. They also measure the quality of images by error-sensitivity. The signal-to-noise ratio is the dimensionless ratio of the signal power to the noise power in a recorded signal. The power of the deterministic signal P_s is given as

$$P_s = \frac{1}{T}\int_0^T s^2(t)dt \tag{5}$$

where T is the interval of observation. The signal-to-noise ratio is typically written as

$$SNR = \frac{P_s}{P_N} = \frac{(A_{signal})^2}{(A_{noise})^2} \tag{6}$$

where P_s is the signal power and P_N is the noise power. A_{signal} is the signal amplitude and A_{noise} the noise amplitude. Since signal-to-noise ratio is often expressed using logarithmtic decibel scale, in decibel, the SNR is expressed as

$$SNR_{dB} = 10\log_{10}\frac{P_{signal}}{P_{noise}} = 10\log_{10}\left(\frac{A_{signal}}{A_{noise}}\right)^2. \tag{7}$$

The concepts of signal-to-noise ratio and dynamic range are closely related. Dynamic range measures the ratio between the strongest and weakest signal on a channel which is actually the noise level. SNR measures the ratio between an arbitrary signal level and noise. Measuring the signal-to-noise ratio requires the selection of a representative reference signal. In image processing, this representative signal is a reference image considered to be noiseless. The numerator of equation (7) is the square of the peak value that the signal could have and the denominator equals the noise power (noise variance). For example, an 8-bit image having values ranging from 0 to 255, for PSNR calculations, the numerator $A^2_{signal} = 255^2$ in all cases. Also,

$$A^2_{noise} = MSE = \frac{1}{N}\sum_{i=1}^{N}|x_i - y_i|^2 = \frac{1}{N}\|E_2\|^2$$

which measures the error between two images. So, we see that the SNR can be reduced to the PSNR in the case of images.

The root mean square error (RMSE) sometimes called the root mean square deviation (RMSD) is frequently used to measure the difference between values predicted by an estimator and the values actually observed from the thing being modeled or estimated. The RMSE of an estimator $\hat{\theta}$ with respect to the estimated parameter θ is defined as the square root of the mean square error

$$RMSE = \sqrt{MSE(\theta)} = \sqrt{E((\hat{\theta} - \theta)^2)} \tag{8}$$

The RMSE measures the square root of the variance if the estimator is not biased. In image processing, the RMSE between two image matrices I, J is given as

$$RMSE(I,J) = \sqrt{MSE(I,J)} = \sqrt{\frac{\sum_{j=1}^{m}\sum_{i=1}^{n}(I_{ij} - J_{ij})^2}{m \times n}} \tag{9}$$

We see from the above argument that the RMSE is related to the MSE because the MSE is a scaled square of the RMSE.

IV. The SSIM

The denoising process is also a structural change process. The MSE-based image quality metrics are not able to measure structural change. For this reason we proceed to study an alternative method of determining quality of denoised images based purely on structural considerations. We then compare the structural methods to the error-sensitivity methods. For the structural approach, we employ the use of the structural similarity index (SSIM) as developed by Zhou Wang, Alan C. Bovik and Eero Simoncelli [3]. First we seek to understand how the SSIM works with a view to applying it to the study of denoised image quality.

We recall that the Minkowski metric does not take the order of the signal samples into consideration. This assumption has grave implications for natural image signals because they are highly structured. It is the ordering and pattern of natural images that give the distinct visual information in images. So the application of a model that takes this fact into account will bring us closer to the true quality of a denoised image. What we need is a metric that senses the structural changes in the image signals.

The luminance of a surface is the product of the illumination and reflectance. However, objects in a scene are independent of illumination. The major impact of illumination change in an image, therefore, is a change in variation of the local luminance and contrast. This variation does not have a significant effect on perceived image quality. Indeed [18] showed that luminance and contrast changes in an image can be separated from structural distortions in the image space. In inage fidelity measurement, retention of image signal structure is important. Luminance change is a nonstructural distortion. Other nonstructural changes include contrast change, gamma distortion and spatial shift. Suppose $\mathbf{x}$ and $\mathbf{y}$ are local image patches taken from the same location of two images, the local SSIM index measures the similarities of three elements of the image patches. These are the luminance similarity $l(\mathbf{x},\mathbf{y})$ which measures the local patch brightness values. The $c(\mathbf{x},\mathbf{y})$ similarity measures determines the local patch contrast values and the $s(\mathbf{x},\mathbf{y})$ determines local patch structural similarity. The forementioned quantites are computed for the whole image and combined together to form the SSIM for the image. The luminance of each signal is estimated as the mean intensity

$$\mu_x = \bar{x} = \frac{1}{N}\sum_{i=1}^{N} x_i \tag{10}$$

The luminance comparison function $l(\mathbf{x},\mathbf{y})$ is then a function of μ_x and μ_y, that is, $l(\mathbf{x},\mathbf{y}) = l(\mu_x,\mu_y)$. We remove the mean intensity from the signal. The resulting signal $\mathbf{x} - \mu_x$ corresponds to the projection of the vector $\mathbf{x}$ onto the hyperplane of $\sum_{i=0}^{N} x_i = 0$. We further use the standard deviation as an estimate of the signal constrast:

$$\sigma_x = \left(\frac{1}{N-1}\sum_{i=1}^{N}(x_i - \mu_x)^2\right)^{\frac{1}{2}} \tag{11}$$

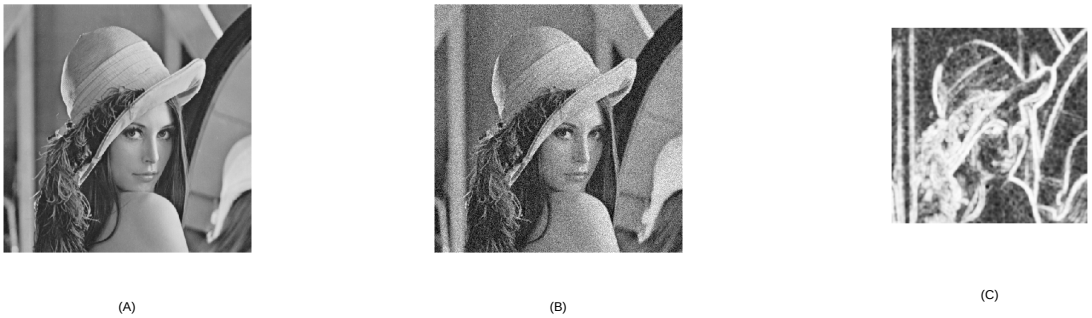

(A) (B) (C)

Fig. 2: (A) Original Pristine Image (B) Image Corrupted with Gaussian Noise (C) The SSIM Image Quality Map of (A) and (B)

The contrast comparison $c(\mathbf{x},\mathbf{y})$ is then the comparison of σ_x and σ_y:

$$c(\mathbf{x},\mathbf{y}) = c(\mu_x,\mu_y)$$

Thirdly, the signal is normalized by its own standard deviation so that the two signals being compared have unit standard deviation. the structure comparison $s(\mathbf{x},\mathbf{y})$ on the normalized signals is:

$$s(\mathbf{x},\mathbf{y}) = s\left(\frac{\mathbf{x}-\mu_{\mathbf{x}}}{\sigma_x}, \frac{\mathbf{y}-\mu_{\mathbf{y}}}{\sigma_y}\right) \tag{12}$$

Finally, the three components are combined to yield an overall similarity measure

$$S(\mathbf{x},\mathbf{y}) = f(l(\mathbf{x},\mathbf{y}), c(\mathbf{x},\mathbf{y}), s(\mathbf{x},\mathbf{y})). \tag{13}$$

The three components do not depend on one another and so the changes in luminance and constrast has no effect on the structures of the object in a scene. We define the functions $l(\mathbf{x},\mathbf{y})$,$c(\mathbf{x},\mathbf{y})$ and $s(\mathbf{x},\mathbf{y})$ as well as the combination of all three functions. Furthermore the similarity measure satisfies the following conditions:

1. Symmetry: $s(\mathbf{x},\mathbf{y}) = s(\mathbf{y},\mathbf{x})$. This means that the order of the input signals should not affect the resulting measurement.
2. Boundedness: $-1 < s(\mathbf{x},\mathbf{y}) \leq 1$. The upper bound indicates how close the two signals are to being identical.
3. Unique maximum: $s(\mathbf{x},\mathbf{y}) = 1$ if and only if $\mathbf{x} = \mathbf{y}$. This perfect score should be achieved only if the compared signals are identical otherwise it should measure any variations that may exist between the images.

The luminance comparison function is defined as

$$l(\mathbf{x},\mathbf{y}) = \frac{2\mu_x\mu_y + C_1}{\mu_x^2 + \mu_y^2 + C_1} \tag{14}$$

In our experiments, $C_1 = 0$ but a common assumption is that $C_1 = (K_1 L)^2$ where L is the dynamic range of the image and $K_1 \ll 1$. The contrast comparison function takes a similar form to the luminance comparison function:

$$c(\mathbf{x},\mathbf{y}) = \frac{2\sigma_x\sigma_y + C_2}{\sigma_x^2 + \sigma_y^2 + C_2} \tag{15}$$

Here also, $C_2 = (K_2 L)^2$ where L is the dynamic range of the image and $K_2 \ll 1$ but we assume that $C_2 = 0$ in our computations. Structure comparison is carried out after luminance subtraction and constrast normalization. The angle between the vectors $\frac{\mathbf{x}-\mu_{\mathbf{x}}}{\sigma_x}$ and $\frac{\mathbf{y}-\mu_{\mathbf{y}}}{\sigma_y}$ each lying in the hyperplane $\sum_{i=1}^{N} x_i = 0$ provides a simple and effective measure that quantifies structural similarity. This corresponds to measuring the correlation coefficient between $\mathbf{x}$ and $\mathbf{y}$. The structure comparison function is defined as:

$$s(\mathbf{x},\mathbf{y}) = \frac{2\sigma_{xy} + C_3}{\sigma_x\sigma_y + C_3} \tag{16}$$

We take $C_3 = 0$. The cross correlation coefficient σ_{xy} is given as

$$\sigma_{xy} = \frac{1}{N-1}\sum_{i=1}^{N}(x_i - \mu_x)(y_i - \mu_y) \tag{17}$$

Finally, we combine the luminance, constrast and structure similarity functions. The result is usually called the structural similarity (SSIM) index. So,

$$SSIM(\mathbf{x},\mathbf{y}) = [l(\mathbf{x},\mathbf{y})]^{\alpha} \cdot [c(\mathbf{x},\mathbf{y})]^{\beta} \cdot [s(\mathbf{x},\mathbf{y})]^{\gamma} \tag{18}$$

where $\alpha > 0$, $\beta > 0$ and $\gamma > 0$ are used to tune the relative importance of the three components. In our experiments we take $\alpha = \beta = \gamma = 1$. So, we have

$$SSIM(\mathbf{x},\mathbf{y}) = \left(\frac{2\mu_x\mu_y + C_1}{\mu_x^2 + \mu_y^2 + C_1}\right) \cdot \left(\frac{2\sigma_x\sigma_y + C_2}{\sigma_x^2 + \sigma_y^2 + C_2}\right) \cdot \left(\frac{2\sigma_{xy} + C_3}{\sigma_x\sigma_y + C_3}\right) \tag{19}$$

where μ_x and σ_y represents the local sample means of $\mathbf{x}$ and $\mathbf{y}$. σ_x and σ_y are the local standard deviations while σ_{xy} is the sample cross correlation of $\mathbf{x}$ and $\mathbf{y}$ after the mean has been removed i.e. the cross correlation of $\mathbf{x} - \mu_{\mathbf{x}}$ and $\mathbf{y} - \mu_{\mathbf{y}}$. In the hyperplane of $\sum_{i=1}^{N} = 0$, the SSIM index compares the vectors $(\mathbf{x} - \mu_{\mathbf{x}})$ and $(\mathbf{y} - \mu_{\mathbf{y}})$ with two independent quantities: the vector lengths and their angles. The angular measure gives an indication of structural distortion.

SSIM indices give a measure of similarity between images. If one of the images is regarded as a reference image, that is of perfect quality, then the SSIM index can ne viewed as an indication of the quality of the other image being compared. Image quality is computed locally rather than globally. The

local statistics μ_x, σ_x and σ_{xy} are computed within a local 8×8 square window. This produces an image quality map (see Fig. 2). The image quality map is combined into a single quality score for the entire image. The local statistics and SSIM are calculated within each window. A drawback of this approach is that the index map exhibits blocking artifacts. To overcome this drawback, the authors in [15] used a circular-symmetric Gaussian weighting function $\mathbf{w} = \{w_i | i = 1, 2, ..., N\}$ with $\sum_{i=1}^{N} w_i = 1$ with the local statistics μ_x, σ_x and σ_{xy} modified by the weighting function $\mathbf{w}$

$$\mu_x = \sum_{i=1}^{N} w_i x_i, \tag{20}$$

$$\sigma_x = \left(\sum_{i=1}^{N} w_i (x_i - \mu_x)^2 \right)^{\frac{1}{2}} \tag{21}$$

and

$$\sigma_{xy} = \sum_{i=1}^{N} w_i (x_i - \mu_x)(y_i - \mu_y). \tag{22}$$

Because of the isotropic property of the Gaussian function, the quality map will exhibit a locally isotropic property also.

The SSIM has worked quite well across a wide variety of applications. Where the MSE-based metrics have failed to provide a good indication of image distortion, the SSIM index has proved to be effective in this respect. For this reason, we employ it in the study of denoised image quality as we see in Fig. 3, the SSIM changes as the denoising parameters change but the MSE remains constant at 255. Here, we see that the MSE do not give a good account of the quality changes in the image. Generally, the SSIM scores are better at representing visual reality.

[18] showed that the SSIM handles texture masking visual effects well. When noise is added uniformly across the image, the visual appearance of the image is more highly degraded in smooth regions of the image. If we use an l_p-norm such as the Minkowski metric to measure the image quality, the measurement is likely to be uniform even though the human eye will observe a degradation of the image. The SSIM scores more in accord with human visual perception than the MSE.

SSIM has been used for evaluating image processing results in applications such as image fusion, image compression, video hashing, etc. Here, we use it to evaluate denoised images. A drawback of the SSIM index is that it is sensitive to translations, scaling and rotation of images. To overcome this, the authors in [15] developed a wavelet domain version of the SSIM called the complex wavelet SSIM (CW-SSIM). If $C_x = \{C_{x,i} | i = 1, 2, ..., N\}$ and $C_y = \{C_{y,i} | i = 1, 2, ..., N\}$ are sets of coefficients extracted from the same spatial location in the same wavelet subbands of two images $\mathbf{x}$ and $\mathbf{y}$, then the CW-SSIM has the following form:

$$\bar{S}(\mathbf{x}, \mathbf{y}) = \bar{m}(C_x, C_y) \cdot \bar{p}(C_x, C_y) = \frac{2 \sum_{i=1}^{N} |C_{x,i}||C_{y,i}| + K}{\sum_{i=1}^{N} |C_{x,i}|^2 + \sum_{i=1}^{N} |C_{y,i}|^2 + K} \cdot \frac{2 |\sum_{i=1}^{N} C_{x,i} C_{y,i}^*| + K}{2 \sum_{i=1}^{N} |C_{x,i} C_{y,i}^*| + K} \tag{23}$$

C^* is the complex conjugate of C and K is a small stabilizer. $\bar{m}(C_x, C_y)$ is determined by the norm of the coefficients. It is maximum when $|C_{x,i}| = |C_{y,i}|$ for all i. $\bar{p}(C_x, C_y)$ is determined by the consistency of phase changes between C_x and C_y. It is maximum when the phase difference between $C_{x,i}$ and $C_{y,i}$ is the same for all i. The phase component effectively measures image structural similarity because the local structure of the image is realized by the relative phase patterns of local image frequencies. Also a constant phase shift of the wavelet coefficients will not change the structure of the local image structure. Just like the SSIM, the CW-SSIM is computed locally from each subband, and then averaged over space and subbands to yield the CW-SSIM index between two images.

V. Noise Models

We consider some noise models that occur in practice. Some are natually occurring such as the gaussian noise; some are sensor-related e.g. photon counting noise and speckle noise. Some kinds of noise arise from processing e.g. quantization and processing. There are additive, multiplicative noise models as well as models which do not fit into these two categories. However, we shall use only additive and multiplicative noise in our experiments. Additive noise is usually intensity-related. Let u be a discrete image and $\delta = (\delta_{i,j})_{i,j}$ be an $n_x \times n_y$ matrix of intensities of independent and identically distributed random variables. If the recorded intensity data are

$$u^\delta = u + d$$

then we speak of additive intensity errors in the image data. Examples are thermal noise, photographic noise and quantization noise. A model for multiplicative noise is given by

$$u^\delta = u \cdot d$$

where $(\delta_{i,j})_{ij}$ is a matrix of values which are independent and identically distributed random variables. The multiplicative noise is understood pointwise i.e. $u_{i,j}^\delta = u_{i,j}\delta_{i,j}$. Poisson noise and salt-and-pepper noise are prominent noise models with a functional dependence of the noise δ on u.

VI. Denoising Models

In our experiments, we use two kinds of noises: additive noise and multiplicative noise. We adopt the use of the Gaussian white noise for additive noise analysis and the salt and pepper noise for multiplicative noise. The choice of these noise types also necessitate that the method of denoising the image should be adapted to the form of the noise as well. For additive noise, we choose the use of the total variation denoising method. The reason for this choice is that the total variation method allows us the possibility to tune the denoising paramaters. This enables us to observe the changes in image quality more easily. We give a brief description of the total variation denoising and its applicability to additive noise restoration.

A. Total Variation Denoising

Image degradation usually results from image acquisition modality and defects in the imaging system or random noise from unwanted signals. Therefore, it is important to choose a noise model that correlates with reality in order to solve a denoising problem successfully. We assume an additive random noise for the total variation denoising method. We model the noise as a Gaussian distribution. Knowing the kind of noise in an image is not not always possible and so some assumptions need to be made. If we assume that $u : \Omega : R^2 \to R$ is an original image and u_0 is the observed image (i.e. the corrupted image from which we wish to obtain u), then we can assume that

$$u_0 = Ru + \eta \tag{24}$$

where η stands for a white Gaussian additive noise and R is a linear operator representing a blur. So, given u_0, we wish to obtain u. This problem is ill-posed because the nature of R is not usually known and there is no direct method of measuring R or η. It can only be formulated as an inverse problem. In accordance with the maximum likelihood principle, we can find an approximation of u from (24) by solving the least squares problem:

$$\inf_u \int_\Omega |u_0 - Ru|^2 dx \tag{25}$$

with Ω as the image domain. (25) is simply a minimization of the MSE. If equation (25) has a minimum, then it must satisfy

$$R^* u_0 - R^* Ru = 0 \tag{26}$$

i.e. $u = R^* u_0$ if $R^* R$ is one-to-one where R^* is the adjoint of R. Because of ill-posedness, obtaining u may not be possible. Because of this, it is necessary to regularize (25) in order to introduce stability into the solution. An idea introduced by Tikhonov and Arsenin (1977) is to overcome ill-posedness by adding a regularization term to (25). Tkhonov and Arsenin considered the following minimization problem:

$$F(u) = \int_\Omega |u_0 - Ru|^2 dx + \lambda \int_\Omega |\nabla u|^2 dx \tag{27}$$

with boundary condition $\frac{\partial u}{\partial N} = 0$. The first term measures the fidelity to the data and the second term is a smoothing term. The experience with using (27) in imaging is that the smoothing term penalizes the edges by smoothing them as well. It is then necessary to reduce the power of the smoothing term. This leads to the Rudin, Osher and Fatemi model. They introduced the use of the total variation functional $\int_\Omega |\nabla u| dx$ instead of the smoothing term in (27). In general, the energy equation can be rewritten as

$$E(u) = \frac{1}{2} \int_\Omega |u_0 - Ru|^2 dx + \lambda \int_\Omega \varphi(|\nabla u|) dx \tag{28}$$

if R is the identity matrix, a denoising will occur, if it is not, a blurring occurs. So, we will take $R \equiv I$. In the smoothing term, we take $\varphi(|\nabla u|) = |\nabla u|$ so that (28) can be rewritten as

$$E(u) = \frac{1}{2} \int_\Omega |u_0 - u|^2 dx + \lambda \int_\Omega |\nabla u| dx \tag{29}$$

where Ω is the domain

We consider

$$E(u) = \frac{1}{2} \int_\Omega |u_0 - Ru|^2 dx + \lambda \int_\Omega \varphi(|\nabla u|) dx \tag{30}$$

as a general form of the total variation regularization of the ill-posed energy equation where φ is a function of $|\nabla u|$. If $E(u)$ has a minimum point u (which is the desired denoised image), then it satisfies the Euler-Lagrange equation

$$R^* Ru - \lambda \text{div} \left(\frac{\varphi'(|\nabla u|}{|\nabla u|} \nabla u \right) = R^* u_0 \tag{31}$$

Equation (31) can be written in an expanded form by formally developing the divergence term

$$R^* Ru - \lambda \left(\frac{\varphi'(|\nabla u|}{|\nabla u|} \right) u_{TT} + \varphi^{''} (|\nabla u|) \, u_{NN} = R^* u_0 \tag{32}$$

where u_{TT} and u_{NN} represent the second derivatives of u in the tangent and normal directions to the image isophotes respectively. At weak intensity variations (low gradients), smoothing occurs in all directions. Assuming the function φ to be regular, this isotropic smoothing condition may be achieved by imposing on φ the following condition: [10]

$$\varphi'(0) = 0, \lim \frac{\varphi'(s)}{s} = \lim \varphi''(s) = \varphi''(0) > 0 \tag{33}$$

Therefore at points where $|\nabla u|$ is small (32) becomes

$$R^* Ru - \lambda \varphi''(0)(u_{TT} + u_{NN}) = R^* u_0 \tag{34}$$

that is

$$R^* Ru - \lambda \varphi''(0)(\Delta u) = R^* u_0 \tag{35}$$

so at these points, u locally has strong regularizing properties in all directions.

In the neighborhood of an edge, the image presents a strong gradient. To preserve the edge, diffusion should occur along the edge and not across it. So the coefficient of u_{NN} in (34) should be eliminated and prevent the coefficient of u_{TT} from vanishing:

$$\lim_{s \to +\infty} \varphi''(s) = 0, \ \lim_{s \to +\infty} \frac{\varphi'(s)}{s} = \beta > 0 \tag{36}$$

When $\varphi(s) = s$ and R is the identity operator, Chambolle [7] has remarked that the minimization of the total variation can be viewed as a projection problem on some convex set. Let $u_{i,j}, (i, j = 1, ..., N)$, be a discrete image and $X = R^{N^2}$ the set of all discrete images of size N^2. In order to define the total variation (TV) of the discrete image, we introduce the gradient

$$\nabla : X \to X \times X :$$

$$(\nabla u)^1_{i,j} = \begin{cases} u_{i+1,j} - u_{i,j} & \text{if } i < N \\ 0 & \text{if } i = N \end{cases} \tag{37}$$

$$(\nabla u)^2_{i,j} = \begin{cases} u_{i,j+1} - u_{i,j} & \text{if } j < N \\ 0 & \text{if } j = N \end{cases} \tag{38}$$

$$(\text{div} p)_{i,j} = (\text{div} p)^1_{i,j} + (\text{div} p)^2_{i,j}$$

A further discretization of the total variation can be found in [7] and [10].

The the discrete TV is the l^1-norm of the vector ∇u by

$$J_{TV}(u) = \sum_{i,j}^{N} |(\nabla u)_{i,j}| \tag{39}$$

J_{TV} is a discretization of the total variation (TV) defined in the continuous setting for a function $u \in L^1(\Omega)$ by

$$J(u) = \sup\left\{ \int_\Omega u(x)\text{div}v(x)dx; v \in C_0^1(\Omega; R^2) | v(x)| \leq 1, \forall x \in \Omega \right\} \tag{40}$$

The equation

$$\inf_{u \in X} \left\{ J_{TV}(u) + \frac{1}{2\lambda}|u_0 - u|_{X^2} \right\} \tag{41}$$

corresponds to the Rudin, Osher and Fatemi model in equation (29).

We introduce the set G and define it as

$$G = \{v \in X; \exists p \in X \text{ s.t. } |p_{i,j}| \leq 1, \forall i,j \text{ s.t. } v = \text{div}p\} \tag{42}$$

The unique minimizer of (41) is given by $u = f - P_{\lambda G}G(f)$ where $P_{\lambda G}G(f)$ is the L^2- othornormal projection of f on the set λG

We proceed to describe the TV denoising algorithm based on duality. Equations (28) and (29), provide a basis for the primal approach but because the solution is degenerate when $|\nabla u| = 0$, the dual approach offers an alternative formulation for effective computational algorithms. The energy model is given as

$$\min_u \int_\Omega |Du| + \frac{\lambda}{2}\int_\Omega (u_0 - u)^2 dx \tag{43}$$

by definition,

$$\int_\Omega |Du| = \sup_{p \in C_c^1(\Omega)} \int_\Omega u \nabla . p dx \tag{44}$$

$\left\{p = (p_1, p_2) | p \in C^1, ||p||_{L^2} < 1\right\}$ using the definition of the TV term, we have

$$\min_u \left(\sup_{p \in C_c^1(\Omega)} \int_\Omega u \nabla . p dx \right) + \frac{\lambda}{2}\int_\Omega (u_0 - u)^2 dx \tag{45}$$

which can be regrouped as

$$\sup_{p \in C_c^1(\Omega)} \min_u \left(\int_\Omega u \nabla . p dx + \frac{\lambda}{2}\int_\Omega (u_0 - u)^2 dx \right) \tag{46}$$

The problem is quadratic in u, therefore it can be solved by setting the gradient of the objective function to zero [1] i.e.

$$u = u_0 - \frac{1}{\lambda}\nabla . p \tag{47}$$

substituting into equation (44) we get the dual formulation

$$\sup_{p \in C_c^1(\Omega)} \left(\int_\Omega u_0 \nabla . p dx - \frac{1}{2\lambda}\int_\Omega (\nabla . p)^2 dx \right) \tag{48}$$

We can take the Lagrangian $(L[p, \mu])$ of the dual problem (46) with the Lagrange multiplier function $\mu = \mu(x)$:

$$L(p, \mu) = \int_\Omega (u_0 \nabla . p - \frac{1}{2\lambda}(\nabla . p)^2 + \frac{\mu}{2}(1 - p^2)) dx \tag{49}$$

Setting the gradient of L with respect to p we get the necessary condition for optimality:

$$-\nabla(u_0 - \frac{1}{\lambda}\nabla . p) - \mu p = 0 \tag{50}$$

The complementary condition of the lagrange multiplier implies that if $|p| = 1$ at the optimum, then $\mu > 0$. If $|p| < 1$, then $\mu = 0$. In any case, $\mu = |H(p)|$ where $|H(p)| = -\nabla(u_0 - \frac{1}{\lambda}\nabla . p)$. Thus, (48) can be written as

$$H(p) - |H(p)|p = 0$$

We use the following time marching scheme

$$p^{n+1} = p^n + \tau\left(H(p^{(n)}) - |H(p^{(n)})|p^{n+1} \right)$$

which leads to the scheme:

$$p^{n+1} = \frac{p^{(n)} + \tau H(p^{(n)})}{1 + \tau |H(p^{(n)})|} \tag{51}$$

Analysis shows that the scheme converges for $0 < \tau \leq \frac{1}{8}$. This is the form in which we use the total variation denosing algorithm in this work.

B. Median Filter

Order statistic filters are spatial filters whose response is based on ranking the values of the pixels contained in the image area delineated by the filter. The result of the ordering determines the filter response. The median filter is an order statistic filter. It replaces the pixel value by the median intensity values in the neighbourhood of that pixel. It is given as

$$f(x, y) = \underset{(s,t) \in S_{xy}}{\text{median}} g(s, t) \tag{52}$$

where S_{xy} is a window in which we take the median values. Median filters provide a very good noise reduction capabilities for certain noise types such as multiplicative noise. A better order statistic filter is the adaptive median filter. The median filter has no regard for image variation from point to point but the adaptive filter filters images based on local image characteristics. For this reason, they do much better than ordinary order statistic filters which fail to perform well when the noise probability density is greater than 0.2 [16]. Adaptive median filtering can handle impulses with noise probabilities much greater than 0.2. Additionally, adaptive median filters seek to preserve detail while smoothing out noise. The adaptive median filter works in a rectangular window and adjusts the size of S_{xy} during operation depending on certain conditions. Let Z_{min} = minimum value of S_{xy}
Z_{max} = maximum intensity value in S_{xy}
Z_{med} = medium intensity value in S_{xy}
Z_{xy} = intensity value at coordinates (x, y)
S_{max} = maximum allowed size of S_{xy}

Reference Image: MSE = 255, SSIM = 1
(a)

Denoised Image: λ = 60,τ = 0.01,
MSE = 255, SSIM = 0.653430
(b)

Denoised Image: λ = 12, τ = 0.01,
MSE = 255, SSIM = 0.892388
(c)

Denoised Image: λ = 2, τ = 0.01,
MSE = 255, SSIM = 0.748494
(d)

Denoised Image: λ = 1, τ = 0.01,
MSE = 255, SSIM = 0.712412
(e)

Denoised Image: λ = 0.5, τ = 0.01,
MSE = 255, SSIM = 0.685501
(f)

Fig. 3: SSIM and MSE Scores for Total Variation Denoised Images

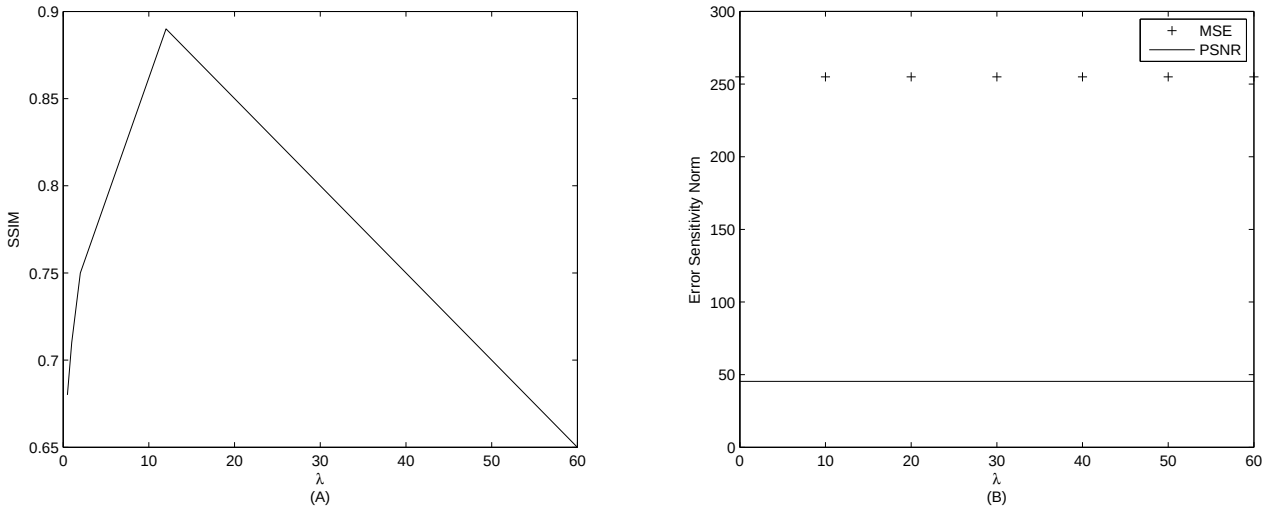

Fig. 4: A Comparison of SSIM and Error Senstivity Norms for TV Denoised Images

The adaptive median-filtering algorithm works in two stages:

`Stage 1`

$A1 = Z_{med} - Z_{min}$

$A2 = Z_{med} - Z_{max}$

`If` $A1 > 0$ `AND` $A2 < 0$ `go to Stage 2`

`Else increase the window size`

`If window size` $\leq S_{max}$ `repeat Stage 1`

`Stage 2`

$B1 = Z_{xy} - Z_{min}$

$B2 = Z_{xy} - Z_{max}$
If $B1 > 0$ AND $B2 < 0$, output Z_{xy}
Else output Z_{med}

The adaptive median filters removes salt and pepper noise, smooth other noise types and reduces distortion. The purpose of the first stage is to determine if the filter output, Z_{med} is an impulse or not. If the condition $Z_{min} < Z_{med} < Z_{max}$ holds, then Z_{med} cannot be an impulse. In this event, the algorithm goes to the second stage and test to see if the point in the center of the window, Z_{xy}, is itself an impulse. If $B1 > 0$ AND $B2 < 0$ is true, then $Z_{min} < Z_{xy} < Z_{max}$ and Z_{xy} cannot be an impulse. In this case, the algorithm outputs the value Z_{xy} unchanged. This helps to minimize distortions in the image. If the condition $B1 > 0$ AND $B2 < 0$ is false, then either $Z_{xy} = Z_{min}$ or $Z_{xy} = Z_{max}$. In either case, the value of the pixel is an extreme value and the algorithm outputs the median value Z_{med} which is not a noise impulse. If the algorithm fails to branch to Stage 2, then the size of the window is increased and Stage 1 is repeated. This continues until a nonimpulse median value is found and branches to Stage 2 or the maximum window size reached in which case the algorithm returns the value Z_{med}. The smaller the noise probability is or the larger S_{max} is, the less likely a premature exit condition will occur. Every time the algorithm outputs a value, the window S_{xy} is moved to the next location in the image. We use a 3×3 window size as a starting window size in our experiments.

VII. Experimental Results

In this section, we show experimental evidence of the arguments proposed in previous sections. First, our interest is in determining if the error sensitivity metrics based on the mean square error (MSE) are sufficient tools in determining the quality of denoised images. For this, we measure the MSE and PSNR of denoised images. On the other hand, we also determine the SSIM index of the images as different parameters of the denoising algorithm are changed. We employ the total variation denoising algorithm in denoising additive Gaussian noise from images and the adaptive median filter for multiplicative noise. Here, the noise type under investigation is the salt and pepper noise. Below we give details of the two approaches showing how they were implemented.

A. Total Variation Approach

The total variation algorithm represented by the time marching algorithm in equation (51) have two parameters λ and τ which determine the denoising process. The algorithm is convergent to a minimum (optimal) value if $0 < \tau \leq \frac{1}{8}$. This proof is provided in [7]. Therefore, it is necessary to keep $\tau \ll 1$ for a good result. As long as τ remains within the interval of convergence, no visible effect can be observed on the quality of the image. In other words, it does not affect the denoising process very much. Because of this fact, we keep $\tau = 0.01$ throughout the experiments. If $\tau > \frac{1}{8}$, convergence is not guarenteed. This does not mean that there will never be convergence but to avoid this uncertainty, we keep τ within the guaranteed interval of convergence. λ is a tuning parameter. The larger λ is the less denoising takes place. Therfore, it is necessary to keep λ small enough to obtain an appropriate denoisng of the image. Small enough means that we should seek the optimal λ for the best denoising of the image. This is indeed a difficult task because there is no unique optimal (best) λ for the best denoising of the image. The best value of λ that gives the best denoising result is image dependent. If the value of λ chosen is greater than the best value for λ, there will be visible noise distortion left in the image after denoising. If the value chosen is less than the optimal λ value, there will be an oversmoothing of the image and its visual quality will fall. In our experiments, we found that even though the visual quality fluctuates, this fact is not captured by the error sensitivity metrics i.e. the MSE and PSNR. The SSIM index of the image however is more sensitive to changes in the values of λ. As we reduce the value of λ from 60 (an arbitrary starting point), the quality of the image continues to improve until the optimal λ value is reached. Thereafter, the SSIM index starts to drop. This happens because of oversmoothing of the image. It is important to understand why this happens. For λ values greater than the optimal λ for denoising the image, the SSIM index is sensitive to the noise distortion in the image and it shows this in the results obtained. When the value of λ drops below the optimal value, oversmoothing begins to occur and this results in blurring. Our previous experiments show that blurring degrades the structural quality of the image. This results in poor SSIM index values. Fig. 1 and Fig. 3 illutrate this. Fig. 4(A) and Fig. 4(B)show the graphs of the relationship between the SSIM, the MSE and the PSNR for total variation denoising. We observe from the graphs that while the MSE and PSNR remain constant for all values of λ, the SSIM index shows that there are changes in the structure of the images. This keeps track of the visual quality of the images as they are denoised at different values of λ. As the value of λ is increased from 0, the quality of the image represented by the SSIM index continues to increase until the optimal value of λ is reached. Thereafter, the quality of the image begins to decline. This optimal value which gives the best denoising result is image dependent, as we have mentioned earlier. The challenge therefore, is to determine an approximation of the best value for λ for each image being denoised. Furthermore, this value of λ is also dependent on the amount of noise present in the image. So at best, determining an appropriate value for λ in any experiment could be a matter of trial and error. What is certain is the pattern of the graph. The improvement and degradation phases of image quality during denoising follow a somewhat linear patterns with a sharp peak representing the best value for λ.

B. Median Filter Approach

Median filters are more effective in removing multiplicative noise than the total variation methods. For this reason, we employ it in the denoising of salt and pepper noise. The noise density was increased from 0 to 1 with increments of 0.1. At each incremented step, we measured the SSIM index, the MSE and the PSNR of the image under increasing noise in Fig. 6B

Fig. 5: Images Distorted by Salt and Pepper Noise and Their MSE and SSIM Scores

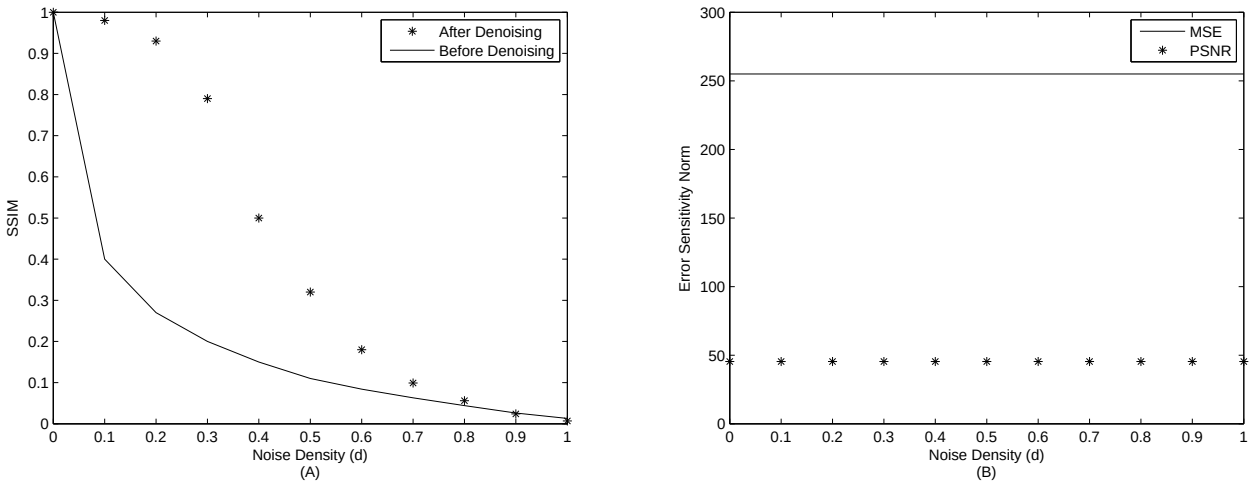

Fig. 6: Salt and Pepper Noise and Error Sensitivity Norms

shows the MSE and the PSNR remained constant but Fig. 6A shows the graph of the structural degradation in the presence of increasing salt and pepper noise. It is interesting to note that the structural degradation of the image under increasing noise density is somewhat exponential in behavior. Fig. 6A also shows the graph of recovery of the image after denoising using the median filter. As the noise density increases to 1, the graphs of the image quality before and after denoising coincide. In other words as noise is increased, the denoising algorithm does little to ameliorate the quality of the image. This is a common phenomenon in image denoising. We also observe that in the case of median filter approach, there does not appear to be an optimal value for which some parameter gives the best denoising possible.

VIII. Conclusion

The error sensitivity metrics have been used to determine the quality of denoised images for a long time. And they have proved to be useful in so far as only nonstructural aspects of image quality are being measured. But the human eye is quite sensitive to structural information. Our experiments have shown that using the error sensitivity metrics alone to determine denoised image quality is not sufficient to describe image quality changes. The use of the SSIM is encouraged to help better ascertain the true quality of a denoised image. The PSNR is commonly used for the purpose of describing denoised image quality. But the PSNR depends on the dynamic range and the MSE of the image. If two images with different dynamic ranges are corrupted with the same amount of noise, the resulting PSNR value will be different because of the difference in dynamic ranges. This is a drawback because this loss of image quality is not caused by some form of external degradation but by the model itself. Thus, it becomes difficult to refer to the quality of a denoised image without reference to its dynamic range. Here, the SSIM offers a better metric for determining the quality of the denoised image since it does not depend on the dynamic range of the image neither does it consider the MSE of the images being compared.

References

[1] Tony F. Chan and Jianchong Shen, *Image Processing and Analysis: Variational, PDE, Wavelet and Stochastic Methods*, SIAM, 2005.

[2] Z. Wang, L. Lu and A.C. Bovik. *Video Quality Assessment based on Structural Distortion Analysis.* IEEE International Conference on Image Processing, Genoa, Italy, Sept. 11-14, 2005.

[3] Z. Wang, A.C. Bovik and E.P. Simoncelli. *Structural Approaches to Image Quality Assessment* in Handbook of Image and Video Processing (Al Bovik, ed., 2nd Edition, Academic Press, 2005.

[4] William P. Ziemer, *Weakly Differentiable Functions*, Springer Verlag, 1989.

[5] J.Bect, Blanc-Feraud, G. Aubert, and A. Chambolle. *A l^1-unified Variational Framework for Image Restoration*, Proceedings of the 8th European Conference on Computer Vision, volume IV, Prague, Czech Republic, springer-Verlag, 2004

[6] Peter Ndajah, Hisakazu Kikuchi, Masahiro Yukawa, Hidenori Watanabe and Shogo Muramatsu. *SSIM Image Quality Metric for Denoised Images*, Advances in Visualization, Imaging and Simulation pp. 53-57. WSEAS Press, 2010.

[7] A. Chambolle. *An Algorithm for Total Variation Minimization and Applications*, Journal of Mathematical Imaging and Vision 20(1-2):89-97, March, 2004.

[8] Takanori Koga, Eiji Uchino, Noriaki Suetake, Genta Hashimoto, Takafumi Hiro and Masanori Matsuzaki. *Speckle Noise Reduction and Edge-Enhancement of Coronary Plaque Tissue in Intravascular Ultrasound Image by Using Anisotropic Diffusion Filter*, International Journal of Circuits, Systems and Signal Processing. Issue 4, Volume 2, 2008 (pp 239-248).

[9] Z. Wang, A.C. Bovik and L. Lu. *Why is Image Quality Assessment Difficult?* IEEE International Conference on Acoustics, Speech and Signal Processing, May, 2002

[10] Gilles Aubert and Pierre Kornprobst. *Mathematical Problems in Image Processing: Partial Differential Equations and the Calculus of Variations, Second Edition*, Springer, 2006.

[11] Ioanu Firoiu, Alexandru Isar, Donna Isar *A Bayesian Approach of Wavelet Based Image Denoising in a Hyperanalytic Multi-Wavelet Context*, WSEAS Transactions on Signal Processing. Issue 4 Volume 6, 2010.

[12] Vincenzo Niola and Giuseppe Quaremba. *Image Denoising and Fuzziness Measures*, Proceedings of the 7th WSEAS International Conference on Neural Networks, Cavtat, Croatia, June 12-14, 2006 (pp 1-6).

[13] Z. Wang and A.C. Bovik. *A Universal Image Quality Index.* IEEE Signal Processing Letters, vol. 9. no.3, pp. 81-84, March 2002

[14] L.Rudin, S. Osher, and E. Fatemi. *Nonlinear Total Variation Based Noise Removal Algorithms*. Physica D, 60: 259-268, 1992.

[15] Z. Wang, A.C. Bovik, H.R. Sheikh and E. P. Simoncelli. *Image Quality Assessment: From error Visibility to Structural Similarity.* IEEE Transactions on Image Processing, vol. 13, no. 4, pp. 600-612, 2004

[16] Rafael Gonzalez and Richard E. Woods, *Digital Image Processing*, Pearson Prentice Hall, 2008.

[17] Hetty Attouch, Giuseppe Buttazzo and Gerard Michaille. *Variational Analysis in Sobolev and BV Spaces.* SIAM, 2006.

[18] Zhou Wang and Alan C. Bovik. *Mean Squared Error: Love it ot Leave it?* IEEE Signal Processing Magazine, January 2009.

[19] Al Bovik, *Handbook of Image and Video Processing*, Academic Press, 2000.

[20] A.I. Tikhonov. *Solutions of Ill-Posed Problems.*Vh Winston, 1977.

[21] Zhou Wang and Alan C. Bovik. *A Universal Image Quality Index.* IEEE Signal Processing Letters, vol. 9 no. 3, pp. 81-84, 2002.

[22] Otmar Scherzer, Markus Grasmair, Harald Grossauer, Markus haltmeier, Frank Lenzen. *Variational Methods in Imaging.* Springer, 2009.

[23] The SSIM Index for Image Quality Assessment. Avalilable: http://ece.uwaterloo.ca/∼z70wang/research/ssim/